European Journal of Mechanics B/Fluids 28 (2009) 753–760

Contents lists available at ScienceDirect

European Journal of Mechanics B/Fluids

journal homepage: www.elsevier.com/locate/ejmflu

Moderate Reynolds number axisymmetric jet development downstream an extended conical diffuser: Influence of extension length

A. Van Hirtum*, X. Grandchamp, X. Pelorson

GIPSA-lab, UMR CNRS 5216, Grenoble Universities, 961 rue de la Houille Blanche, BP 46, 38402 Saint-Martin d'herès, France

ARTICLE INFO

Article history:
Received 30 September 2008
Received in revised form
30 April 2009
Accepted 8 May 2009
Available online 28 May 2009

Keywords:
Round jet
Single sensor anemometry
Initial conditions
Self-similarity
Velocity statistics
Upper airways

ABSTRACT

Low-velocity (bulk velocity of 4.4 m/s) and moderate Reynolds (7350) axisymmetrical jet development is studied by hot-film single sensor anemometry. The jet issues from a conical convergent-divergent diffuser with uniform extension (diameter 25 mm). Decreasing the length-to-diameter ratio of the extension tube from 20 down to 0.4 is shown to alter severely the mean velocity profile at the tube outlet from Blasius to top-hat whereas turbulence intensities increases from 6 up to 50%. Next, the influence of the initial velocity profile at the tube outlet on axisymmetrical jet development is assessed. The velocity development exhibits a self-similar far field characteristic for axisymmetrical jet development. Although, the jet centerline decay constant increases and the jet spreading rate decreases as length-to-diameter ratios are increased from 0.4 up to 7.2 for which the initial centerline velocity decreases. Therefore, scaling of the centerline decay constant and inverse scaling of the spreading rate with initial centerline velocity U_0 or initial velocity Reynolds number Re_0 reported for moderate Reynolds numbers and low initial turbulence levels [18,22] does not hold as the turbulence level exceeds a threshold value in the range 12–27%. In addition, the influence of initial conditions on near and far field turbulence properties is shown. A transition in near field behaviour is observed for length-to-diameters around 3.6. Flow and geometrical configurations under study are relevant to e.g. upper airway flow.

1. Background and objectives

The time-averaged spatial velocity development of an embedded axisymmetric free jet issuing from a nozzle with diameter d has been the subject of numerous theoretical modelling, experimental as well as numerical studies. As a consequence, its global characteristics are well understood, e.g. Refs. [25,30]. In general, the time-averaged turbulent jet flow mixing region is divided into three parts: an initial near field region downstream the exit, followed from $4d$ up to $8d$ by a transition region and a self-preserving far field region further downstream [11]. Approximate solutions describing the far field flow evolution assume the mean centerline velocity U_c to decrease proportional to x^{-1}, where x indicates the streamwise direction from the tube exit. The centerline decay rate K depends on the transverse velocity profile, initial mean centerline velocity U_0 and tube diameter d [25,30]. Consequently, for given d and initial mean bulk velocity U_b, i.e. for given Reynolds number Re_b or given initial momentum $M_0 = \pi d^2 U_b^2/4$, universal behaviour is expected to appear when scaled with respect to the near field extent indicated by the virtual origin x_0. The extent of the near field is further determined by the end of the potential core along the centerline commonly denoted x_p. Inside the potential core, U_c is assumed to equal initial mean centerline velocity U_0 [25,30].

Despite the described universal behaviour, the influence of initial conditions and geometry on axisymmetrical jet development is put forward from analytical arguments, numerical simulations as well as experimental evidence. In, e.g. Refs. [9,10] it is shown analytically that the averaged equations of motion for a number of flows admit to more general similarity solutions that retain a dependence on both the Reynolds number and the initial conditions. Consequently, decay rate constants, K and the virtual origin, depend on conditions at the tube outlet. Those analytical findings were in agreement with earlier experimental results of [16,22,32,12] illustrating among others the influence of initial conditions on the development of coherent structures and consequently on the spreading rate for Reynolds numbers $Re > 10^4$. More recent experimental studies confirmed these earlier findings by putting into evidence the influence of initial conditions as well as nozzle geometry features: e.g. nozzle diameter [18], nozzle shape [26,21], boundary layer thickness [14,28], exit velocity profile [1,34], exit grid [6] and Reynolds number [24,27]. In addition, the influence of the initial velocity profile at the tube exit is shown by means of numerical simulations [4].

* Corresponding author. Tel.: +33 4 76 57 45 37; fax: +33 4 76 57 47 10
E-mail address: annemie.vanhirtum@gipsa-lab.inpg.fr (A. Van Hirtum).

0997-7546/$ – see front matter © 2009 Elsevier Masson SAS. All rights reserved.
doi:10.1016/j.euromechflu.2009.05.004

List of symbols

x	longitudinal distance from exit plane (m)
y	transverse distance from centerline (m)
x_0	virtual origin (m)
x_p	end of the potential core (m)
d	inner tube diameter (m)
$d_{1,2}$	auxiliary diameter (m)
L_t	subscript $t \in \{1, 3, 11, 18, 50\}$ indicates extension tube length (cm)
$L_{a,b}$	auxiliary length (m)
$U_i(x,y)$	instantaneous velocity (m/s)
$U(x,y)$	mean velocity (m/s)
$U_c(x)$	centerline mean velocity (m/s)
U_0	centerline mean velocity at tube outlet (m/s)
U_b	bulk velocity near tube outlet (m/s)
$u(x,y)$	velocity fluctuation $U_i - U$ (m/s)
u_1	x component of fluctuating velocity (m/s)
u_2	y component of fluctuating velocity (m/s)
$y_{1/2}$	transverse half-width such that $U(x, y_{1/2}) = U_c(x)/2(m)$
$u'(x,y)$	second moment of u or root mean square (rms)
$S_u(x)$	third moment of u or skewness $S_u \equiv \langle u^2 \rangle^3/\sigma^3$
ν	kinematic viscosity of air (m^2/s)
Re_0	Reynolds number based on d and U_0, i.e. $U_0 d/\nu$ (dimensionless)
Re_b	Reynolds number based on d and U_b, i.e. $U_b d/\nu$ (dimensionless)
K	centerline decay rate (dimensionless)
K'	centerline decay rate, i.e. $K' = KU0/Ub$ (dimensionless)
M_0	initial momentum (m^4/s^2)
S	spreading rate $S \equiv dy_{1/2}/dx$ (dimensionless)
α	Gaussian function parameter (dimensionless)
$\nu_T(x, y)$	turbulent viscosity (m^2/s)
η	similarity variable $\eta \equiv y/x - x_0$ (dimensionless)
$\widehat{\nu}_T(\eta)$	normalised turbulent viscosity profile $\widehat{\nu}_T(\eta) \equiv \nu_T/U_c(x)y_{1/2}(x)$ (dimensionless)
n, C_1, C_2	model parameters (dimensionless)
ω	frequency (s^{-1})
k	normalised wavenumber $k \equiv \omega \cdot d/U_c(x)$ (dimensionless)
$E(k)$	velocity spectra of u

Most of the cited studies deal with Reynolds numbers $\geq 10^4$. Nevertheless, in particular jets associated with moderate Reynolds numbers, $Re < 10^4$, appear to be sensitive to initial conditions [9,18]. Experimental studies dealing with the influence of diameter d and initial mean velocity U_0 on the centerline velocity decay of axisymmetric jets with uniform initial outlet profile at moderate Reynolds numbers are presented in [22,18]. Those studies show that the centerline velocity decay coefficient decreases and the half-width spread angle increases for decreasing outlet Reynolds numbers. Moreover in [18] it is concluded that the velocity decay coefficients are best correlated by the nozzle centerline velocity at the outlet U_0. Both studies [22,18] dealt with ASME Standard Long Radius Nozzles with diameters 0.1524, 0.0758 and 0.0401 m for Reynolds numbers of order $Re \approx 10^4$ and turbulence intensities below 9%. Obviously, data for moderate Reynolds numbers, $Re < 10^4$ and non-standard nozzle geometries are less studied despite their potential applications.

Among applications of particular interest here are configurations relevant to the human upper airways [23]. The lack of velocity flow measurements issuing from upper airway configurations was e.g. pointed out by Howe et al. in their study on fricative sibilants [13]. In the current study moderate Reynolds numbers Re of order of 10^3 and relatively short extended convergent-divergent diffusers with length-to-diameter ratios $L_t/d < 20$ are considered [23]. Such geometrical configurations, although a crude approximation, are relevant to flow through the human upper airways since: 1) a narrowed upstream passage is present in the upper airways, e.g. at the larynx (glottis) and the lips, or naturally created in the oropharynx during articulation [13,8,19,31] and 2) a typical vocal tract length for a newborn and adult is 7 and 18 cm respectively [8,19,31]. Further variation of the geometrical length scale L_t, corresponding to varying the extension length is e.g. due to morphology, pathology or articulation during speech production.

Therefore, in the following the spatial jet development is searched for given initial momentum $M_0 = \pi d^2 U_b^2/4$, i.e. constant tube diameter $d = 25$ mm and constant initial bulk velocity $U_b = 4.4$ m/s resulting in moderate Reynolds $Re = 7350$ and low Mach number flow of order 10^{-2}. The influence of extension tube length L_t on the velocity profile at the tube outlet and on the resulting jet development is searched. Jet development is measured by scanning the velocity field with hot-film single sensor anemometry from the tube exit up to 20 times extension tube diameter d.

2. Experimental setup

The jet is generated in a flow facility consisting of an air compressor (Atlas Copco GA7) followed by a manual valve and pressure regulator (Norgren type 11-818-987) enabling to provide constant air pressure. A uniform duct of diameter 1 cm connects the pressure regulator with a thermal mass flow meter (TSI 4040) with accuracy 0.1 l/min. The mass flow meter is connected to a conical diffuser by a uniform duct of diameter 1 cm and length 20 cm. Finally, a uniform circular extension tube with fixed diameter $d = 25$ mm and varying length L_t is added downstream the diffuser. Experiments are performed at a constant mass flow rate of 130 l/min corresponding to $U_b = 4.4$ m/s and consequently $Re_b = 7350$. The jet at the exit of the extension tube propagates in a free field at rest. The diffuser has a 14° convergent portion of length 2 cm followed by a 22° divergent portion of length 5 cm. The ratio of outlet and minimum diameter yields 5. The outlet diameter of the diffuser equals the extension tube diameter d. The assessed extension tube lengths yield 1, 3, 9, 18 and 50 cm corresponding to length-to-diameter ratio $L_t/d \in \{0.4, 1.2, 3.6, 7.2, 20\}$. The geometry of diffuser and downstream extension tube is schematically detailed in Fig. 1. The rectangular free field chamber has height, width and length corresponding to 120, 120 and 112 times the outlet diameter d.

A constant temperature anemometer system (IFA 300) is used in order to perform flow velocity measurements. The hot-film is calibrated against mean velocities given by the flow meter. A fourth order polynomial law is fitted to the anemometers output voltage

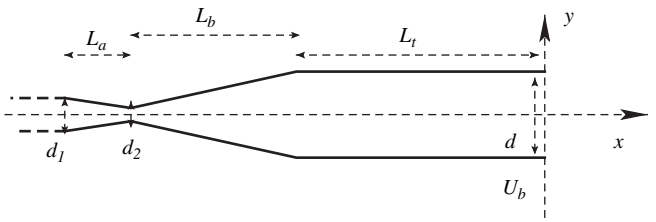

Fig. 1. Schematic overview of the geometry of diffuser ($d_1 = 1$ cm, $d_2 = 0.5$ cm, $L_a = 2$ cm, $L_b = 5$ cm) and extension tube of variable length $L_t \in \{1, 3, 9, 18, 50\}$ cm and fixed diameter $d = 2.5$ cm and flow condition $U_b = 4.4$ m/s or $Re_b = 7350$. The x dimension follows the centerline of the tube in the flow direction and y corresponds to the transverse direction.

in order to convert measured voltage to velocity with an accuracy of 0.1 m/s [5]. Longitudinal and transverse velocity profiles are obtained by moving a single sensor hot film (TSI 1201-20) with a diameter of 50.8 μm and a working length of 1.02 mm using a two-dimensional stage positioning system (Chuo precision industrial co. CAT-C, ALS-250-C2P and ALS-115-E1P). The accuracy of positioning in the longitudinal and transverse direction yields 4 and 2 μm respectively. Longitudinal velocity profiles along the centerline are measured from the tube exit up to 20d downstream. Transverse profiles are assessed near the tube exit and at 1.6, 3.2, 4, 4.8, 6.4, 8, 12 and 16 times d. The applied step size in the longitudinal direction yields $\Delta x = 1$ mm from the tube exit up to 12.7d and $\Delta x = 1$ cm further downstream. The step size in the transverse direction yields $\Delta y = 1$ mm. At each position, velocity data are sampled at 30 kHz during 3 s consecutively.

3. Initial conditions

The influence of L_t on the initial transverse velocity profile at the tube outlet at $x/d < 0.01$ is illustrated in Fig. 2(a) and (b). The normalised mean (U/U_0) and fluctuating (u'/U_0) part of the transverse velocity profiles near the tube exit are shown for all assessed tube lengths. As a benchmark, Blasius's solution expected to occur for long pipe flow is indicated in Fig. 2(a), i.e. $U/U_0 = (1 - 2y/d)^{1/n}$ with $n = 7$. The initial mean velocity profile is seen to evolve from almost top-hat for $L_t/d = 1.2$ towards Blasius's profile as the ratio L_t/d is increasing. Note, that this does not hold for $L_t/d = 0.4$ where no initial top-hat profile could be observed due to the proximity of the diffuser. Nevertheless, the ratio 0.4 is not omitted since data are relevant with respect to flow through the upper airways, e.g. when dealing with the production of consonants [31].

Besides the mean velocity profile, L_t/d is seen to influence the initial turbulence level to a large extent as shown in Fig. 2(b). The turbulence level at the center of the tube exit, $y/d = 0$, decreases from 50 down to 6% of U_0 when L_t/d is increased from 0.4 up to 20. The decrease in initial turbulence level for increasing L_t/d is due to the presence of the narrow upstream passage with small inner diameter causing high turbulence level at the exit of the conical diffuser. The turbulence production decreases downstream the diffuser in the extension tube while pipe flow is developing. Consequently, the initial turbulence level at the tube outlet decreases as the tube length L_t/d increases. The turbulence level of 6% for the largest L_t/d ratio approaches values reported in literature for long pipe flow [34].

The influence of the initial conditions on jet development is assessed in the next section.

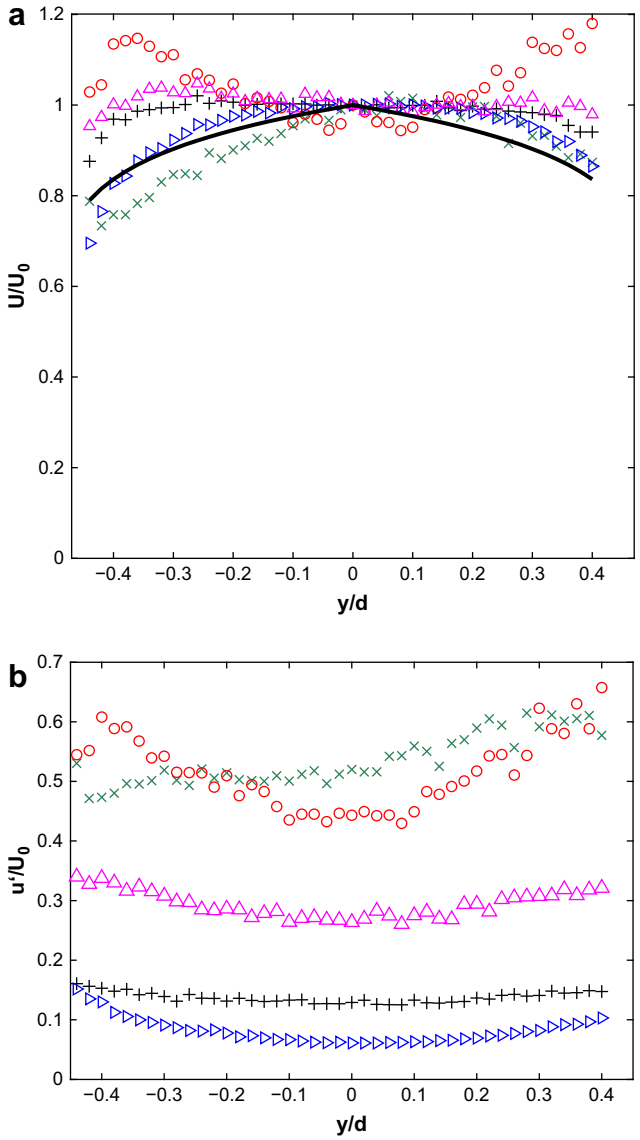

Fig. 2. Initial conditions at tube exit ($x/d < 0.01$) for L_t/d 0.4 (×), 1.2 (○), 3.6 (Δ), 7.2 (+) and 20 (▷): a) normalised mean velocity U/U_0 and Blasius profile (fullline) b) normalised rms of velocity u'/U_0.

4. Characterisation of spatial jet development

4.1. Centreline velocity development

Observed mean longitudinal centerline velocity profiles downstream the tube exit for different L_t/d are illustrated in Fig. 3. The centerline velocity U_c is seen to decrease proportional to x^{-1}, which is expected for a self-similar axisymmetric jet [25,30]. Consequently, the centerline velocity profile is modelled as [25,18]:

$$\frac{U_0}{U_c} = \frac{1}{K}\left(\frac{x - x_0}{d}\right). \tag{1}$$

The near field extent is accounted for by considering a virtual origin x_0, deduced from the measured data as the intercept of the decay line with the abscissa x/d, i.e. $U_0/U_c(x_0/d) = 0$. Resulting centerline decay rates K, virtual origins x_0 and initial conditions are summarised in Table 1. Inverse normalised longitudinal mean centerline velocities *ce:small-caps*>U_0/U_c compensated for the self-similar law are illustrated in Fig. 3.

In general, the decay rate K is seen to increase with L_t/d. The K values tend towards reported centerline decay rates for a long pipe jet in literature $K = 6.7$, $K = 6.5$, $K = 6.3$, e.g. Refs. [7,34,4]. The experimentally derived decay rates $K(L/d \approx 1180) = 6.5$, $K = 5.9$ and $K = 6.7$ reported in e.g. Refs. [34,15,7], are found for flows at considerable higher Re_b, i.e. at 86,000 and 24,000 respectively. The numerically obtained mean centerline velocity decay values, $K = 5.9$ for initial top-hat and $K = 6.3$ for initial parabolic velocity profile, are again obtained for much higher $Re_b = 24{,}000$ [4]. The dependence of the centerline velocity decay factor K on the Reynolds number for $0.5 \leq U_0 \leq 30$ as $K \sim Re_0$ was shown since the fifties although details of the relationship remained unclear [22]. More recently, [18] showed the correlation of the decay factor K with the initial centerline velocity U_0 resulting in a decrease of K for $U_0 < 6$ m/s. The current measurements are in good agreement with data for $K(U_0)$ described in [18] for $L_t/d = 20$ and $L_t/d = 7.2$. Although, for $L_t/d < 7.2$, K decreases while U_0 increases and

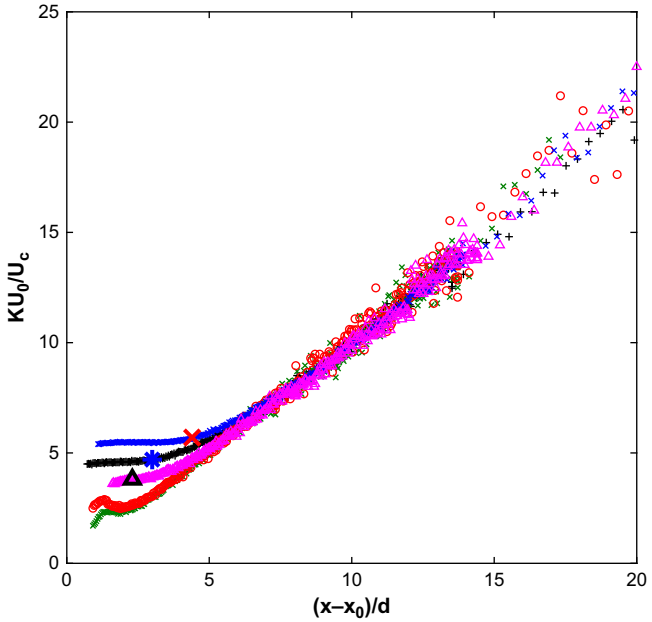

Fig. 3. Inverse normalised longitudinal mean centerline velocities U_0/U_c compensated for the self-similar law: L_t/d 0.4 (×), 1.2 (○), 3.6 (Δ), 7.2 (+) and 20 (▷). The potential core x_p in the self-similar representation is indicated for L_t/d 3.6 (Δ), 7.2 (*) and 20 (▷).

therefore the current data do not agree with the correlation $K(U_0) \sim U_0$ described in [18]. This is due to high initial turbulence levels for $L_t/d < 7.2$, exceeding 25%, whereas the data of [18,22] has turbulence levels smaller than 9%.

Since the initial mean centerline velocity is no longer a good basis for correlation when the turbulence intensity is high, i.e. exceeding a threshold level in between 12 and 27% for the current experiments, it is interesting to consider a different correlation for the centerline decay. Expressing the centerline decay in function of the bulk velocity U_b is of interest since universal self-similar behaviour is expected as the set $\{d, U_b\}$ is not altered based on momentum conservation. An expression for the U_b/U_c is easily derived from Eq. (1) by introducing decay rate $K' = KU_0/U_b$. Moreover, the ratio U_0/U_b in K' is a simple way to account for the shape of the initial mean velocity profile, i.e. Blasius or top-hat.

Resulting K' values are summarised in Table 1. For $L_t/d = 0.4$, an increase in K' reflects the influence of the jet issuing from the inlet diameter d_2 of the upstream diffuser on the jet development due to a severe increase in U_0/U_b. For $L_t/d > 0.4$, K' is seen to increase with L_t/d, as was the case for K. Consequently, accounting for the shape of the initial mean velocity profile by considering the ratio U_0/Ub does not explain the scaling of the decay constant as $\sim 1/U_0$ instead of $\sim U_0$. The decrease in K' and K for smaller L_t/d is therefore mainly related to increasing initial turbulence intensities which favours centerline velocity decay.

Table 1
Experimentally estimated decay rates $K(U_0)$, virtual origin x_0, potential core length x_p as function of L_t/d and decay rates $K'(U_b)$ for $Re_b \approx 7350$. Initial centerline conditions U_0 (m/s) and $100u'/U_0$ are indicated as well.

L_t/d	U_0	$u'/U_0 \times 100$	K	x_0/d	x_p/d	K'
0.4	7.9	52	1.7	−0.92	–	3.1
1.2	4.6	44	2.5	−0.92	–	2.6
3.6	3.8	27	3.6	−1.6	0.7	3.2
7.2	3.8	12	4.5	−0.72	2.3	3.9
20	4.1	6	5.4	−1.1	3.3	5.1

The potential core length x_p of the jet is estimated from the measured mean centerline velocities assuming that inside the potential core $U_c \geq 0.95U_0$ [2]. Resulting x_p, given in Table 1 and indicated in Fig. 3, are seen to increase with L_t/d. Consequently, larger x_p values are associated with more developed pipe flow. This is in agreement with literature, although the maximum value of $x_p = 3.3d$ is below values reported for long pipe flow ranging from 4.7 up to $7.7d$ [2]. Again, values denoted in literature are obtained for much higher Reynolds numbers and initial mean exit velocities U_0 than is the case in this study, e.g. 22,500 in Ref. [2].

The development of turbulence along the centerline is illustrated in Fig. 4(a). The development of turbulence downstream the tube outlet for $L_t/d = 20$ corresponds to increasing u'/U_c in the potential core due to collapsing of the surrounding mixing regions until an asymptotic u'/U_c value is reached. The collapse of the mixing regions towards the end of the potential core, and associated u'/U_c, is also retrieved for L_t/d ratios 7.2 and 3.6. Although, the increase is preceded by an intensity decrease reflecting reduced turbulence production along the centerline until the collapse of the mixing region becomes notable. Remark that for $L_t/d = 1.2$ and 0.4 no increase in u'/U_c occurs due to the absence of a potential core

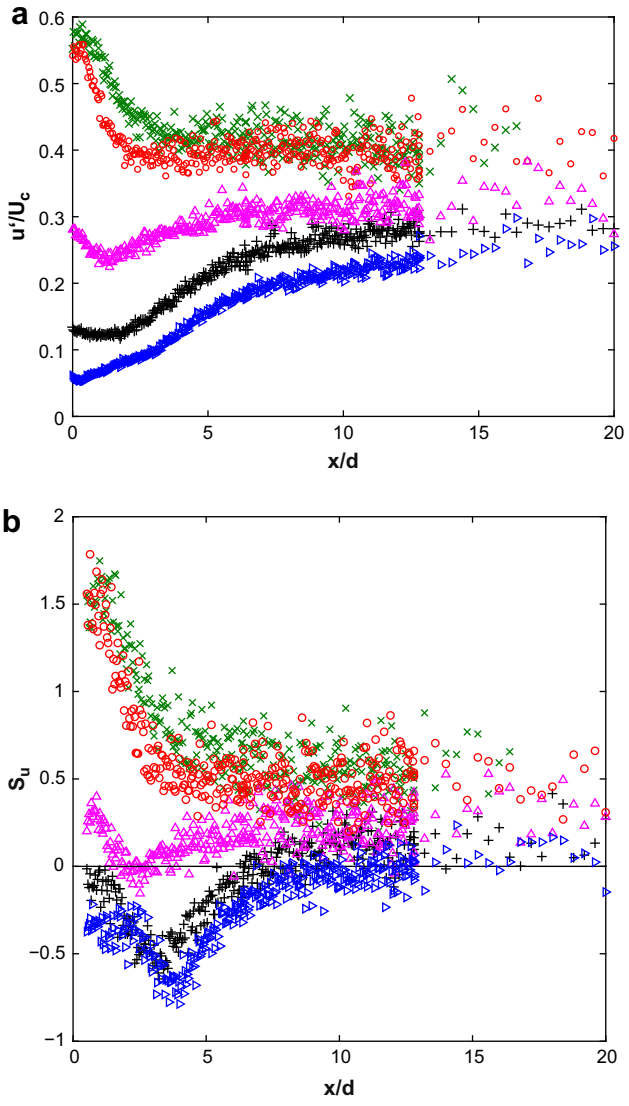

Fig. 4. a) Normalised centerline rms of velocity u'/U_c and b) velocity skewness S_u along the centerline for: L_t/d 0.4 (×), 1.2 (○), 3.6 (Δ), 7.2 (+) and 20 (▷).

although the initial decrease is observed. The different initial rms conditions at the outlet and consecutive different development of the mixing layers results in increased asymptotic u'/U_c values from 0.25 up to 0.4 when the initial turbulence level increases. The asymptotic levels $0.2 \leq u'/U_c \leq 0.3$ found for $L_t/d \geq 3.6$ correspond to the range reported in previous studies for initial turbulence levels below 10% [20,34]. Remark that the downstream distance to reach asymptotic values decreases for increasing L_t/d. For all L_t/d asymptotic values are reached for $x/d \geq 8$.

Turbulence development is further characterised by its higher statistical moments. The skewness S_u, shown in Fig. 4(b), is expected to approach values associated with a Gaussian distribution in case self-similarity is reached, i.e. $S_u = 0$ [25,3,17]. Although, statistics are indeed seen to tend towards Gaussian skewness for all assessed L_t/d, $S_u = 0$ is seen to fit in particular for larger L_t/d associated with initial turbulence levels below 12%. This suggests that the flow exhibits more coherent underlying structures and hence that the flow is less random in case the turbulence level exceeds 25%.

Important initial turbulence intensities at the outlet cause turbulent energy to be convected from regions of large intensity to regions of smaller intensity. Such gradients of turbulence intensity are associated with important positive skewness, $S_u > 0$. This is seen in the near field for the high turbulence levels larger than 40% for $L_t/d = 0.4$ and 1.2. The skewness S_u decreases downstream due to the decrease in turbulence intensity u'/U_c until self-similarity is reached.

For initial turbulence levels below 15% the skewness is seen to evolve from nearly Gaussian $S_u = 0$ to non-Gaussian values $S_u < 0$ and back to $S_u \approx 0$ in the self-similar field. This initial departure from Gaussian indicates the transition of the flow from the initial low turbulence level to the asymptotic level in the self-similar field. In the first portion the shear layers develop and large scale structures are formed until the end of the potential core is attained resulting in $S_u < 0$. Downstream the potential core turbulent energy is transferred until self-similarity is reached resulting in a decrease of $|S_u|$ as was observed for high initial turbulence levels. The initial skewness of the intermediate ratio $L_t/d = 3.6$ yields ± 0.4 due to the initial turbulence level and decreases further downstream since the turbulence level decreases as was the case for the short ratios associated with high turbulence. Downstream the potential core end turbulence is developed until self-similarity is reached, which is associated with a slight increase in skewness, so that the final S_u is in between Gaussian and the level retrieved for short extension ratios.

In general, statistical turbulence properties along the centerline confirm the occurrence of self-similarity and isotropy for the centerline velocity in the far field. The near field behaviour reflects the initial rms values at the outlet and the consecutive development of the jet, which are significantly altered by varying L_t/d.

4.2. Transverse velocity development

The expected self-similar profile for a round free jet is modelled by the normalised Gaussian function centered around zero [25],

$$\frac{U(x,y)}{U_c(x)} = e^{-\alpha\left(\frac{y}{x}\right)^2}, \tag{2}$$

where α is related to the spreading rate of the jet as

$$\alpha = \frac{\ln(2)}{S^2} \tag{3}$$

Spreading rates reported in literature for a round jet issuing from a nozzle with diameter 2.54 cm and Reynolds number of order 10^4 yields $\alpha = 94$ [33] and $\alpha = 78$ [15].

The normalised mean transverse velocity profiles, for all assessed L_t/d and $x/d > x_p/d$, are self-similar when expressed against the similarity variable $y/y_{1/2}$ as illustrated in Fig. 5. Remark the influence of the potential core at x/d for $L_t/d = 20$.

The dependence of the transverse spreading $y_{1/2}$ on L_t/d for all assessed x/d is summarised in Fig. 6. A linear growth rate of $y_{1/2}/d$ is observed as function of x/d for all L_t/d downstream the potential core extension, i.e. $x/d > x_p/d$. The derived experimental spreading rates S are seen to decrease towards $S = 0.083$ as L_t/d increases. This is illustrated in Fig. 7. As a benchmark literature values $S = 0.086$ and $S = 0.094$, corresponding to $\alpha = 94$ and 78 in Eq. (2), are indicated. The spreading rate $S = 0.086$ approximates experimental values for $L_t/d \geq 7.2$, i.e. $S = 0.083$.

Remark that all mean transverse velocity profiles can be modelled with the Gaussian function given in Eq. (2). The model parameter α is easily derived from the experimentally obtained spreading rates from Eq. (3).

Fig. 8 illustrates the transverse fluctuating velocity profile normalised by the mean centerline velocity u'/U_c at $x/d = 1.6$. Development of the shear layers with increasing x/d is observed for $Lt/d \geq 3.6$. For the lowest ratios $Lt/d < 3.6$ the flow is turbulent at the exit and consequently no shear layer development is observed.

4.3. Turbulent viscosity

The concept of turbulent viscosity for a gradient-transport model is shown to be relevant on the jet centerline where turbulence production in the shear layers is negligible and turbulence is due to the transport of the mean and turbulent motion [29,26,25]. A turbulent viscosity $\nu_T(x,y)$ can be estimated from the spreading rate S and half-width $y_{1/2}$ as [25]:

$$\nu_T(x,y) = y_{1/2}(x)U_c(x)\widehat{\nu}_T(\eta) = \frac{S}{8(\sqrt{2}-1)}. \tag{4}$$

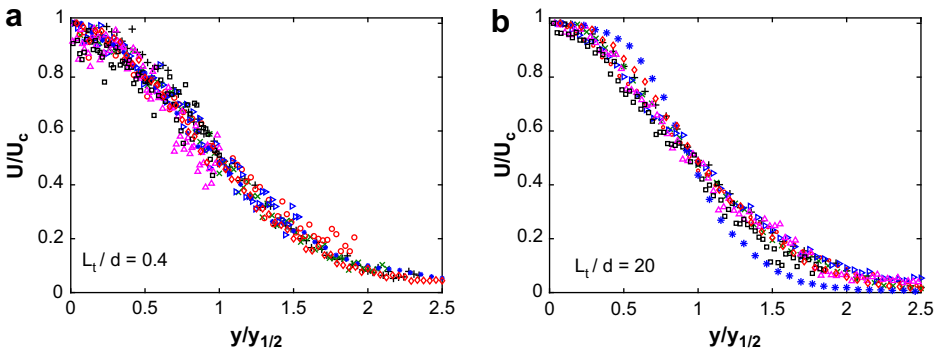

Fig. 5. Similarity representation of transverse normalised axial mean velocity profiles U/U_c for x/d 1.6 (*), 3.2 (◇), 4 (+), 4.8 (×), 6.4 (○), 8 (▷), 12 (Δ), 16 (□).

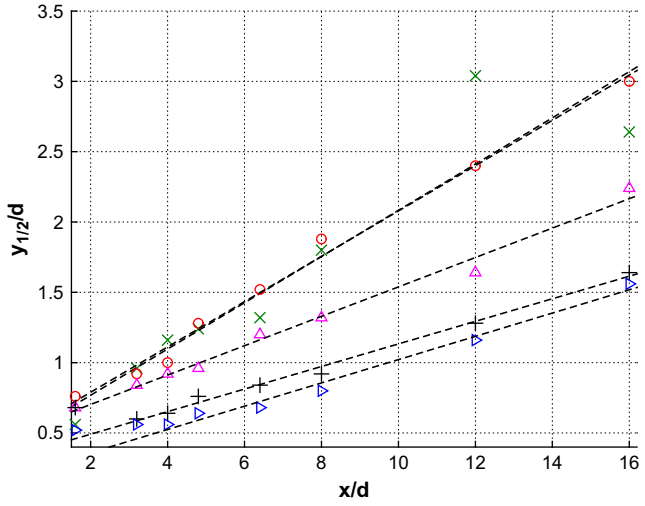

Fig. 6. Normalised half-width $y_{1/2}/d$ for L_t/d 0.4 (×), 1.2 (○), 3.6 (Δ), 7.2 (+) and 20 (▷).

The turbulent viscosity obtained from Eq. (4) for different L_t/d and downstream distances x/d is exemplary illustrated in Fig. 9. For a given downstream distance x/d the estimated value ν_T is shown to be constant within the experimental error, for $L_t/d \geq 3.6$. Moreover it is seen that ν_T decreases with x/d in the same way when $L_t/d \geq 3.6$.

The assumption of turbulent viscosity $\nu_T(x,t)$ allows to estimate the shear stresses,

$$\overline{u_1 u_2} = -\nu_T \frac{\partial U}{\partial y}, \tag{5}$$

from the mean velocity field [25]. The position and magnitude for the positive and negative shear stress peaks, and therefore also the slopes between negative and positive peaks, are expected to depend on L_t/d due to e.g. $S(L_t/d)$ in Eq. (4). As an exemplar, estimated shear stresses for all assessed L_t/d at $x/d = 1.6$ are illustrated in Fig. 10. It is seen that due to the derivative in Eq. (5) the variance on the data is amplified resulting in a noisy shear stress estimation. This is in particular the case for small L_t/d ratios. The estimated noisy shear stresses suggest indeed shifts in peak position and amplitude to occur, but do not allow an accurate quantification. Shear stresses should be derived directly from two-component velocity measurements. Nevertheless, the estimated shear stresses are of the order of magnitude reported in literature for high

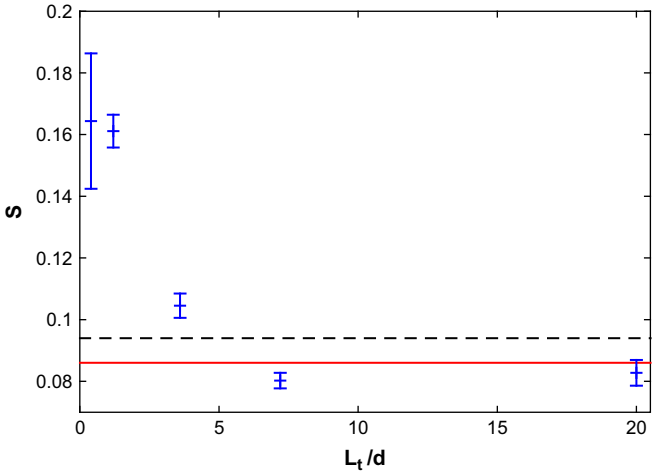

Fig. 7. Spreading rates $S(L_t/d)$, 0.094 (dotted) and 0.086 (full) are derived from [15] and Gaussian function Eq. (2) with $n = 94$.

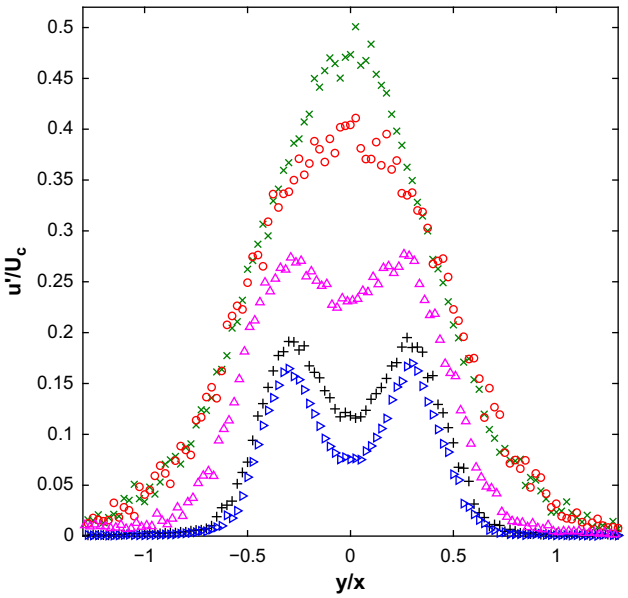

Fig. 8. Normalised transverse rms velocity at $x/d = 1.6$ for L_t/d 0.4 (×), 1.2 (○), 3.6 (Δ), 7.2 (+) and 20 (▷).

Reynolds number flows [26,25] indicating that mixing by momentum transfer by the shear stresses $\overline{u_1 u_2}$ occurs at a similar rate as for high Reynolds number flow.

4.4. One-dimensional energy spectra

The one-dimensional velocity spectra of the turbulent velocity inform on the energy scales. A simple power law is applied in order to model the energy spectra $E(k)$ as:

$$E(k) = \frac{C_1}{\left(1 + \frac{k}{C_2}\right)^n}, \tag{6}$$

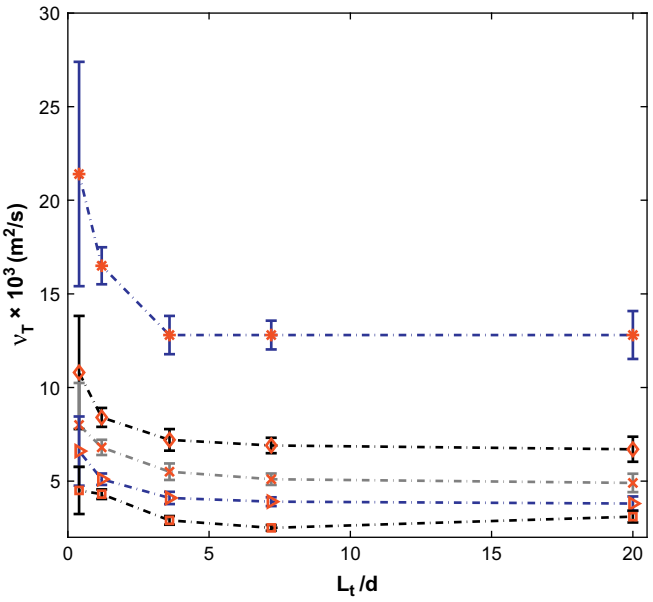

Fig. 9. Experimental turbulence viscosity $\nu_T(L_t/d)$ at x/d 1.6 (*), 3.2 (◇), 4.8 (×), 8.0 (▷) and 16 (□).

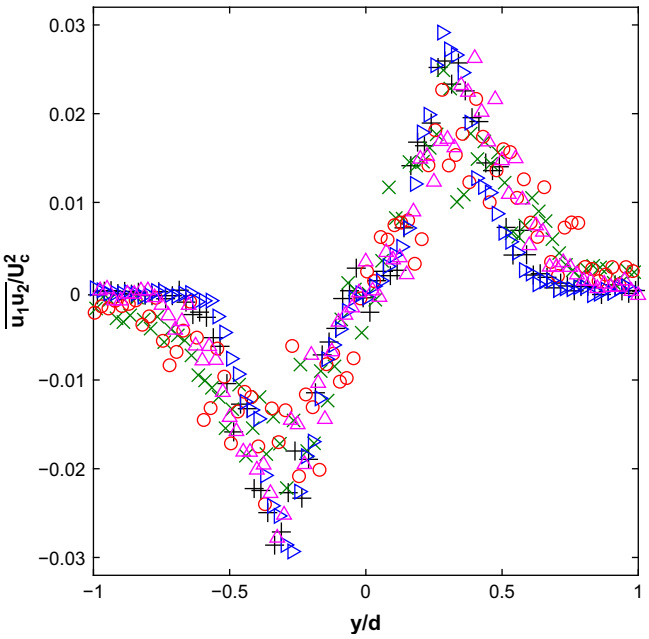

Fig. 10. Normalised estimated shear stresses at $x/d = 1.6$ for L_t/d 0.4 (×), 1.2 (○), 3.6 (Δ), 7.2 (+) and 20 (▷).

with dimensionless wavenumber $k = \omega \cdot d/U_c(x)$ and $C_{1,2}$ model constants. The exponent $n = 5/3$ describes the inertial portion of the spectra corresponding to Kolmogorovs law [25]. The one-dimensional velocity spectra at $x = 1.6d$ and maximum shear stress position as seen in Fig. 8 are illustrated for all assessed L_t/d in Fig. 11. The energy spectra are modelled following Eq. (6) with $C_2 = 0.07$ for all spatial positions and all L_t/d whereas C_1 varies with spatial position. Kolmogorovs power law $E(k) \sim k^{-5/3}$ describes well the inertial part of the spectrum. Note that the extent of the inertial part, described by Kolmogorovs power law $E(k) \sim \sim k^{-5/3}$, is limited due to the moderate value of the Reynolds number [25]. The different development of the shear layers for different L_t/d is in particular reflected in the decay part.

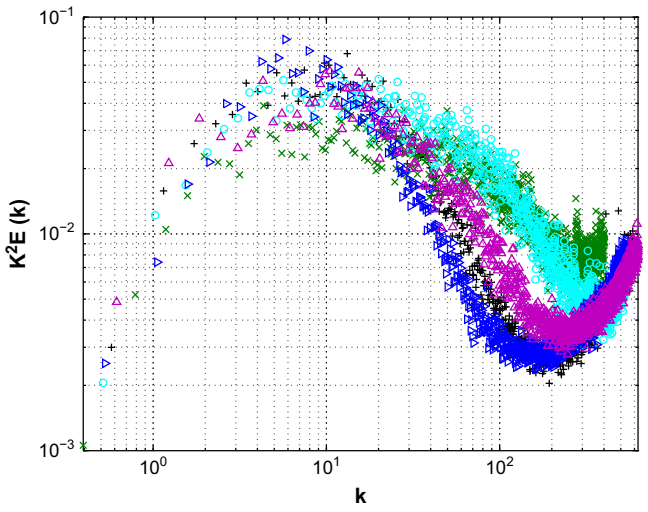

Fig. 11. One-dimensional velocity spectra at $x = 1.6d$ at maximum shear stress position for Lt/d 0.4 (×), 1.2 (○), 3.6 (Δ), 7.2 (+) and 20 (▷) where $k = \omega d/U_c(x)$ denotes the dimensionless wavenumber.

5. Conclusion

The diffusion of a jet downstream a convergent-divergent extended conical diffuser with outlet diameter $d = 2.5$ cm, is considered for fixed bulk Reynolds number (7350). The length of the extension tube is shortened so that length-to-diameter ratios vary from 20 down to 0.4. Flow and geometrical conditions are in a range relevant to airflow through the upper airways as e.g. for human speech production. Mean and turbulent velocity characteristics are estimated from single sensor anemometry along the centerline (0 up to 20d) and at several transverse distances (0 up to 16d).

The following conclusions are made:

I) Both the shape of mean (Blasius to top-hat) and fluctuating portion (rms 6–50%) of the initial velocity profile at the tube outlet are severely altered as the ratio L_t/d decreases reflecting the influence of the upstream diffuser on initial conditions. Consequently, for the range of flow and geometrical conditions studied, varying the extension length downstream a convergent-divergent diffuser is a natural way to vary initial conditions. Since the assessed flow and geometries are in the range relevant to upper airway flow during speech production, initial conditions and in particular initial turbulence levels are likely to exhibit important variations depending on the articulator's positions. This should be confirmed on human 'in-vivo' speakers.

II) With respect to centerline and transverse mean velocity modelling it is shown that self-similar models can be applied regardless the initial conditions. Nevertheless, established relationships between common model parameters such as the centerline velocity decay $K \sim U_0$ and the spreading rate $S \sim 1/U_0$ are inversed as the initial turbulence level increases from 12 up to 27%. Additional data in this turbulence range should be considered to establish a region for which the relationship $K \sim U_0$ is inversed due to high initial turbulence levels which favours velocity decay. Moreover, additional data might allow the relationship of the centerline velocity decay with U_0 to be extended to account for the initial turbulence level. With respect to upper airway geometries and flow conditions, self-similar jet models can be applied although parameters need to be adapted depending on the initial turbulence level and initial mean velocity U_0.

III) Comparing transverse and centerline turbulence statistics, i.e. rms and skewness, for all assessed extension tubes illustrates the difference in shear layer development. Centerline turbulence statistics yields asymptotic values for $x/d \geq 8$ for which the value depends on the initial turbulence level and so on L_t/d. The difference in shear layer development is also observed in the one-dimensional velocity spectrum. The spectra exhibit a common inertial range of limited extent due to the moderate Reynolds number followed by a decay range which depends on L_t/d in accordance with the difference in turbulence development.

IV) Since a gradient-transport model is generally assumed to hold near the centerline of an axisymmetrical jet, turbulent viscosity near the centerline is estimated in order to assess the shear stresses in this region as well as to obtain a qualitative estimation away from the centerline. Two-component velocity measurements are required to obtain an accurate measurement of the shear stresses in order to validate the shear stress estimations over a large range of initial turbulence intensities. The current turbulent viscosity and shear stress estimations provide a qualitative estimation which might be applied in speech production modelling.

Acknowledgements

The support of the French Rhône-Alpes Region (CIBLE 2006) and Agence Nationale de la Recherche (ANR-07-JCJC-0055) is gratefully acknowledged.

References

[1] R. Antonia, Q. Zhao, Effect of initial conditions on a circular jet, Exp. Fluids 31 (2001) 319–323.
[2] S. Ashforth-Frost, K. Jambunathan, Effect of nozzle geometry and semi-confinement on the potential core of a turbulent axisymmetric free jet, Int. Comm. Heat Mass Transfer 23 (1996) 155–162.
[3] G. Batchelor, The Theory of Homogeneous Turbulence. Cambridge Science Classics, 1999.
[4] B. Boersma, G. Brethouwer, F. Nieuwstadt, A numerical investigation on the effect of the inflow conditions on the self-similar region of a round jet, Phys. Fluids 10 (1998) 899–909.
[5] H. Bruun, Hot-Wire Anemometry, Oxford Science Publications, New York, 1995.
[6] P. Burattini, R. Antonia, S. Rajagopalan, M. Stephens, Effect of initial conditions on the near-field development of a round jet, Exp. Fluids 37 (2004) 56–64.
[7] E. Ferdman, M. Otugen, S. Kim, Effect of initial velocity profiles on round jets, J. Propul. Power 16 (2000) 676–686.
[8] W. Fitch, J. Giedd, Morphology and development of the human vocal tract: a study using magnetic resonance imaging, J. Acoust. Soc. Am. 106 (1999) 1511–1522.
[9] W. George, Recent Advances in Turbulence, Hemisphere, New York, 1989, Chapter: The self-preservation of turbulent flows and its relation to initial conditions and coherent structures, pp. 39–73.
[10] W. George, The decay of homogeneous isotropic turbulence, Phys. Fluids A 4 (1992) 1492–1509.
[11] M. Goldstein, Aeroacoustics, McGraw-Hill, New York, 1976.
[12] E. Gutmark, C. Ho, Preferred modes and spreading rates of jets, Phys. Fluids 26 (1983) 2932–2938.
[13] M. Howe, R. McGowan, Aeroacoustics of [s], Proc. R. Soc. A 461 (2005) 1005–1028.
[14] A. Hussain, M. Zedan, Effects of the initial condition on the axisymmetric free shear layer: effects of the initial momentum thickness, Phys. Fluids 20 (1978) 1100–1112.
[15] H. Hussein, S. Capp, W. George, Velocity measurements in a high Reynolds number momentum conserving axisymmetric turbulent jet, J. Fluid Mech. 258 (1994) 31–75.
[16] S. Ling, C. Wan, Decay of isotropic turbulence generated by a mechanically agitated grid, Phys. Fluids 15 (1972) 1363.
[17] J. Lumley, Stochastic Tools in Turbulence, Dover Books, New York, 1970.
[18] T. Malmstrom, A. Kirkpatrick, B. Christensen, K. Knappmiller, Centreline velocity decay measurements in low-velocity axisymmetric jets, J. Fluid Mech. 246 (1997) 363–377.
[19] R. McGowan, Perception of synthetic vowel exemplars of 4-year-old children and estimation of their corresponding vocal tract shapes, J. Acoust. Soc. Am. 120 (2006) 2850–2858.
[20] J. Mi, G. Nathan, R. Luxton, Centreline mixing characteristics of jets from nine differently shaped nozzles, Exp. Fluids 28 (2) (2000) 93–94.
[21] J. Mi, P. Kalt, G. Nathan, C. Wong, PIV measurements of a turbulent jet issuing from round sharp-edged plate, Exp. Fluids 42 (2007) 625–637.
[22] H. Nottage, Report on Ventilation Jets in Room Air Distribution, Tech. Rep., Case Inst. of Technology, Cleveland, Ohio, 1951.
[23] X. Pelorson, A. Hirschberg, R. Van Hasselt, A. Wijnands, Y. Auregan, Theoretical and experimental study of quasisteady-flow separation within the glottis during phonation. Application to a modified two-mass model, J. Acoust. Soc. Am. 96 (1994) 3416–3431.
[24] W. Pitts, Reynolds number effects on the mixing behavior of axisymmetric turbulent jets, Exp. Fluids 11 (1991) 135–141.
[25] S. Pope, Turbulent Flows, Cambridge University Press, 2005.
[26] W. Quinn, Upstream nozzle shaping effects on near field flow in round turbulent free jets, Eur. J. Mech. B/Fluids 25 (2006) 279–301.
[27] G. Romano, R. Antonia, Longitudinal and transverse structure functions in a turbulent round jet: effect of initial conditions and Reynolds number, J. Fluid Mech. 436 (2001) 231–248.
[28] S. Russ, P. Strykowski, Turbulent structure and entrainment in heated jets: the effect of initial conditions, Phys. Fluids 5 (1993) 3216–3225.
[29] J. Sautet, D. Stepowski, Dynamic behavior of variable-density, turbulent jets in their near development fields, Phys. Fluids 7 (2) (1995) 2796–2806.
[30] H. Schlichting, K. Gersten, Boundary Layer Theory, Springer Verlag, Berlin, 2000.
[31] K. Stevens, Acoustic Phonetics, MIT Press, London, 1998.
[32] C.F.I. Wygnanski, B. Marasli, On the large scale structures in two-dimensional, small-deficit, turbulent wakes, J. Fluid Mech. 168 (1986) 31–71.
[33] I. Wygnanski, H. Fiedler, Some measurements in the self preserving jet, J. Fluid Mech. 38 (1969) 577–612.
[34] G. Xu, R. Antonia, Effect of different initial conditions on a turbulent round free jet, Exp. Fluids 33 (2002) 677–683.